AL-DOPED SILICENE NANORIBBONS IN AN EXTERNAL ELECTRIC FIELD

Hoang Van Ngoc (1)
(1) Thu Dau Mot University
Corresponding author's email: ngochv@tdmu.edu.vn

DOI: 10.37550/tdmu.EJS/2026.01.705

Article Info

Volume: 8
Issue: 1
March: 2026
Received: Sep. 4th, 2025
Accepted: Jan. 15th, 2026
Page No: 165-175

Abstract

Silicene nanoribbons (SiNRs), as one-dimensional derivatives of silicene, exhibit highly anisotropic charge transport and hold significant promise for future nanoelectronics applications. In this work, we systematically investigate the structural stability and electronic properties of hydrogen-passivated SiNRs doped with aluminum using first-principles density functional theory calculations performed with the VASP package. Several possible Al substitutional doping configurations are examined, among which three representative geometries-top, valley, and 1-1 arrangements-are identified as energetically stable, while other configurations undergo severe structural distortions or bond breaking during structural relaxation. Formation energy analysis indicates that the 1-1 alloy configuration is the most thermodynamically favorable due to the symmetric distribution of Al dopants and a balanced local bonding environment. Electronic structure calculations reveal that pristine hydrogenated SiNRs are narrow-gap semiconductors with a band gap of approximately 0.325 eV, whereas all stable Al-doped systems undergo a transition to semi-metallic behavior. This electronic transformation originates from the incorporation of group-III aluminum atoms, which introduce hole carriers and shift the Fermi level, leading to enhanced electrical conductivity. In addition, the tunability of the electronic properties is further explored under a constant external electric field of 0.15 eV/Å, demonstrating additional control over the electronic response of the doped nanoribbons. These results highlight aluminum doping, in combination with external electric-field modulation, as an effective strategy for tailoring the electronic characteristics of silicene nanoribbons and suggest promising opportunities for the design of low-dimensional materials with controllable transport properties for advanced nanoelectronics and optoelectronic applications.

Keywords: Al; configurations; DFT; electric field; one-dimensional system; silicene nanoribbons.

1. Introduction

Low-dimensional materials have become an important research focus in condensed matter physics and nanotechnology due to their remarkable structural versatility and tunable electronic properties. Their development has enabled continuous scaling of

electronic components toward smaller, lighter, and more energy-efficient devices. Among these materials, graphene has been widely regarded as the foundation of the modern two-dimensional (2D) materials revolution. Following graphene's success, its silicon - based counterparts - germanene and silicene - have attracted growing interest for their compatibility with existing semiconductor technologies (Takeda & Shiraishi, 1994; Guzmán-Verri & Lew Yan Voon, 2007).

Silicene, in particular, is a 2D honeycomb structure formed by silicon atoms exhibiting a characteristic buckling that differentiates it from planar graphene. This buckled geometry gives silicene a unique combination of Dirac-like electronic dispersion and field-tunable band structure (Cahangirov et al., 2009; Lebègue & Eriksson, 2009). Its structural flexibility also enables growth on different substrates, leading to modifications in its electronic behavior ranging from semimetallic to semiconducting phases (Vogt et al., 2012; Fleurence et al., 2012). Such tunability underpins the increasing interest in silicene for next-generation nanoelectronics and optoelectronic applications (Drummond et al., 2012; Ezawa, 2012).

Beyond monolayer silicene, silicene nanoribbons (SiNRs) have emerged as promising one-dimensional (1D) derivatives due to quantum confinement effects and edge-dependent electronic features (Ding & Ni, 2009; Kara et al., 2012). Their reduced dimensionality enhances sensitivity to structural modifications, external fields, and chemical functionalization. Hydrogen-passivated SiNRs, in particular, exhibit controllable band gaps and structural stability suitable for nanoscale transistor architectures. Modifying SiNRs through heteroatom doping has become a widely explored strategy for engineering their electronic structure, carrier mobility, and magnetic properties.

From a theoretical standpoint, density functional theory (DFT) remains the standard computational framework for predicting the ground-state behavior of low-dimensional materials with high accuracy and reasonable computational cost. The Vienna Ab Initio Simulation Package (VASP) is one of the most reliable tools for DFT-based simulations of structural and electronic properties across a wide range of 2D and 1D systems (Kresse & Furthmüller, 1996; Kresse & Joubert, 1999). In addition, external electric fields have been shown to significantly influence band alignment, charge redistribution, and magnetic responses in silicene-based materials, enabling fine control over their electronic characteristics (Ezawa, 2013).

Motivated by these findings, this study focuses on aluminum-doped, hydrogen-passivated silicene nanoribbons subjected to a constant external electric field. Aluminum doping introduces localized electronic states and modulates carrier concentration, while the applied electric field further enhances tunability. By examining different Al substitutional sites and concentrations, we aim to elucidate their combined impact on the structural stability and electronic properties of SiNRs. The insights obtained from this work contribute to the design of functional silicene-based materials for future nanoelectronics applications.

2. Research Methods

All first-principles calculations in this work were performed within the framework of density functional theory (DFT) as implemented in the Vienna Ab Initio Simulation Package (VASP) (Kresse and Furthmüller, 1996; Kresse and Joubert, 1999). The interactions between valence electrons and ionic cores were described using the projector augmented-wave (PAW) method. The standard PAW potentials supplied with VASP were employed for Al, Si, and H atoms. Exchange-correlation effects were treated using the generalized gradient approximation (GGA) in the Perdew-Burke-Ernzerhof (PBE) functional, which has been widely validated for low-dimensional silicon-based systems.

A plane-wave cutoff energy of 500 eV was adopted to ensure good convergence of total energies and electronic structures. Owing to the one-dimensional periodicity of the silicene nanoribbons, Brillouin-zone sampling was performed using a Monkhorst-Pack k-point mesh of 1×1×11 along the ribbon axis, while a single Γ-point was used in the non-periodic directions. Convergence tests with respect to k-point sampling were carried out to confirm that this k-point density is sufficient for accurately describing the total energies, band structures, and density-of-states features reported in this work. A vacuum region of at least 20 Å was introduced in the lateral directions to avoid spurious interactions between periodic images. Structural optimizations were performed until the residual forces on each atom were smaller than 0.001 eV/Å, and the total energy convergence criterion was set to 10^{-6} eV.

Hydrogen-passivated armchair silicene nanoribbons (SiNRs) were constructed as the pristine reference systems. Aluminum substitution was introduced by replacing one or more silicon atoms at different lattice positions within the nanoribbon, depending on the configuration considered. For each configuration, full structural relaxation was carried out to obtain the most energetically favorable geometry. The relative stability of the modified nanoribbons was evaluated using formation-energy calculations based on the optimized structures.

To investigate the influence of an external electric field, a uniform electric field with a strength of 0.15 eV/Å was applied perpendicular to the plane of the nanoribbon using the dipole correction scheme implemented in VASP. This method enables reliable assessment of electric-field-induced modifications in charge distribution, electronic band structure, and total energy while eliminating artificial interactions arising from periodic boundary conditions.

Formation energy:

$$\Delta E_f = E_t - nE_{Si} - nE_{Al} \quad (1)$$

where, E_t is the total energy of the system; n and m are the number of Al and Si atoms, respectively.

E_{Si}, E_{Al} denote the chemical potentials of Si and Al, taken as the total energies per atom of bulk Si (diamond structure) and bulk Al (fcc structure), respectively:

$$E_{Si} = \frac{E_{total}(\text{Si bulk})}{N_{Si}} \; ; E_{Al} = \frac{E_{total}(\text{Al bulk})}{N_{Al}}$$

3. Results and Discussion

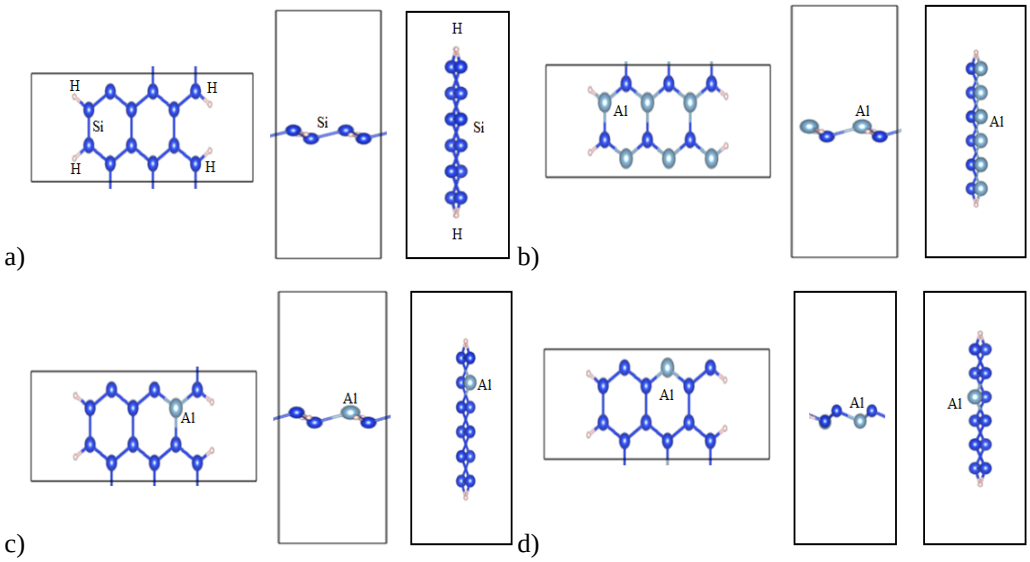

Figure 1. Configurations: (a) Pristine SiNRs, (b) 1-1 alloy configuration, (c) Top-configuration, (d) Valley-configuration.

Source: Author, 2025

In this study, all calculations were carried out using density functional theory (DFT), with specific VASP input parameters selected to ensure reliable structural relaxation and accurate evaluation of the electronic response under an external electric field. The parameter ISIF = 3 was employed, enabling simultaneous relaxation of both atomic positions and cell shape during the optimization process.

The initial pristine configuration of the hydrogen-passivated silicene nanoribbon consists of twelve silicon atoms forming the backbone of the ribbon, with four hydrogen atoms saturating the open edge bonds (Figure 1a). After full structural relaxation, this configuration is found to be stable, exhibiting a total energy of -68.965 eV, which serves as a reference for assessing the relative energetics of the doped systems. All optimized structures in this work show no imaginary forces or lattice distortions, confirming that the selected computational parameters are adequate for maintaining structural stability throughout the calculations.

The 1-1 alloy configuration, shown in Figure 1b, corresponds to a heavily doped structure in which six silicon atoms are replaced by six aluminum atoms within the unit cell, while the remaining atoms include six silicon atoms in the backbone and four hydrogen atoms at the edges. Despite the high doping concentration, the system relaxes into a stable geometry with a total energy of -72.343 eV, which is significantly lower than that of the pristine ribbon. This decrease in total energy indicates that aluminum incorporation at these sites is energetically favorable under the given conditions.

Table 1. The energies and fenergies of formation (ΔE_f)

Systems	E_t(eV)	E_{pr}(eV)	E_{Si} (eV)	E_{Al}(eV)	ΔE_f (eV)
1-1 alloy	-72.343	-68.965	-0.152	-0.174	-3.246
Top	-69.593	-68.965	-0.152	-0.174	-0.496
Valley	-69.673	-68.965	-0.152	-0.174	-0.576

Source: Author, 2025

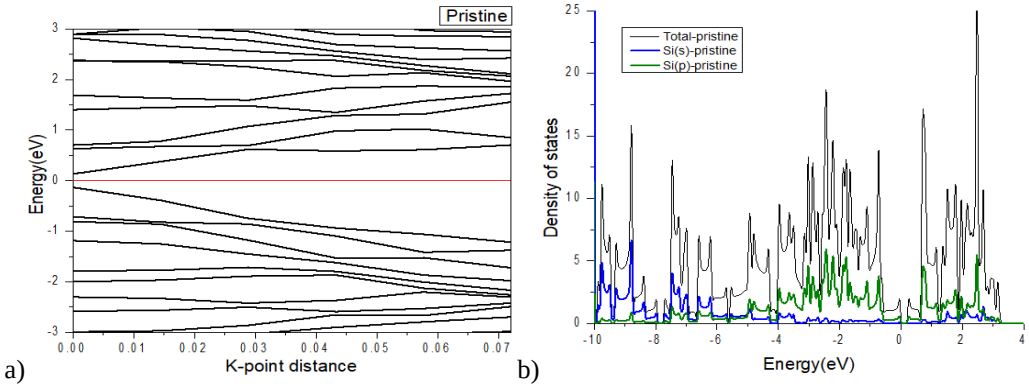

Figure 2. Electronic band structure and density of states of pristine system.

Source: Author, 2025

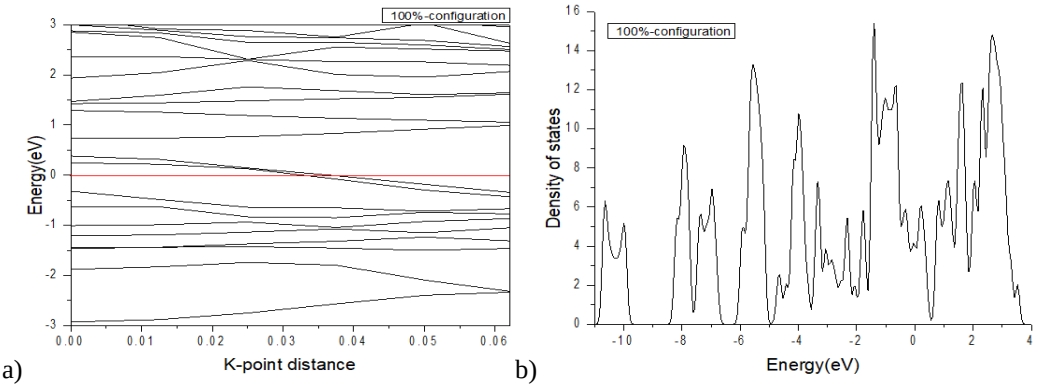

Figure 3. Electronic band structure and density of states of 1-1 alloy system.

Source: Author, 2025

The top configuration, illustrated in Figure 1c, involves substitution of a single silicon atom by an aluminum atom at the upper surface of the nanoribbon. This structure also remains stable after optimization, with a total energy of -69.593 eV, slightly lower than that of the undoped ribbon. The modest reduction in energy suggests a mild stabilization effect from isolated Al doping at this site.

Similarly, the valley configuration (Figure 1d), where the Al atom is positioned at a lower-buckled site within the silicene sublattice, is found to be structurally stable. Its optimized total energy is -69.673 eV, which is lower than both the pristine system and the top configuration, indicating that doping at valley sites is energetically more favorable than at top sites.

Table 1 summarizes the calculated formation energies for the 1-1, top, and valley configurations. Among the examined structures, the 1-1 alloy configuration exhibits the highest magnitude of formation energy, which reflects its energetic favorability despite the substantially higher dopant concentration. The relatively large formation energy suggests that the incorporation of multiple Al atoms into the silicene nanoribbon is thermodynamically favorable under the selected computational conditions. This also indicates that the local bonding environment created by the distributed Al atoms contributes to the stabilization of the lattice rather than disrupting the integrity of the ribbon.

In contrast, the top and valley configurations, each containing a single dopant atom, show lower formation energies, consistent with their reduced level of structural perturbation. Between these two, the valley-doped structure exhibits a slightly more negative formation energy, implying that Al substitution at the lower-buckled site is more stable than at the upper-buckled site. This trend is consistent with the asymmetric buckling inherent in silicene, where valley sites often provide a more favorable bonding environment for substitutional impurities.

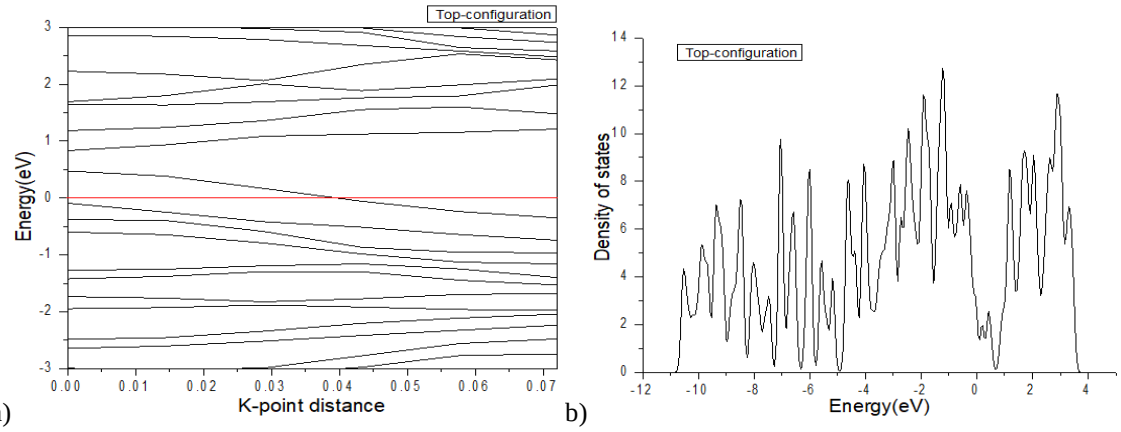

a) b)

Figure 4. Electronic band structure and density of states of top doped system.

Source: Author, 2025

The electronic band structure of the pristine hydrogen-passivated silicene nanoribbon (Figure 2) reveals that the system is semiconducting, exhibiting a narrow band gap of approximately 0.325 eV. This relatively small gap is characteristic of low-dimensional silicon-based materials and suggests moderate electronic tunability under external perturbations. The corresponding partial density of states (PDOS) further clarifies the orbital contributions to the electronic structure. As shown in Figure 2, the s-states are primarily localized in the deep valence-energy region (blue curve), while the p-states dominate near the band edges (green curve). The p-orbital character near the Fermi level is typical of puckered silicene, in which sp^2/sp^3 hybridization governs the frontier electronic states.

Figures 3-5 display the electronic band structures and DOS for the 1-1, top, and valley configurations, respectively. In all three cases, the introduction of Al atoms dramatically alters the original semiconducting behavior. The band gap completely vanishes, and a small overlap emerges between the conduction-band minimum and the valence-band maximum around the Fermi level. This behavior is indicative of a semi-metallic electronic structure, where the system supports charge transport via both electrons and holes.

The semi-metallic nature of the doped systems can be attributed to the substitution of silicon (a group-IV element) by aluminum (a group-III element). Because Al possesses one fewer valence electron than Si, its incorporation introduces hole-like carriers into the lattice, effectively shifting the Fermi level and enhancing p-type conduction. This explains why all doped configurations transition from a semiconductor to a semi-metal after Al substitution.

When comparing the different doping geometries, the 1-1 alloy configuration shows a distinct electronic behavior due to its significantly higher doping concentration. In the

valence band, away from the Fermi level, the distribution of electronic states is notably more diffuse than in the top and valley configurations. This redistribution of states reflects enhanced perturbation of the Si backbone and increased hybridization between Al and Si atoms.

The projected density of states (PDOS) analysis provides clear insight into the electronic origin of the semi-metallic behavior observed in the 1-1 alloy configuration. As shown in the PDOS for Si atoms, the valence band region well below the Fermi level (from approximately -10 to -4 eV) is dominated by Si(s) states, while the states closer to the Fermi level are primarily associated with Si(p) orbitals. This indicates that the Si framework largely retains its sp-hybridized bonding characteristics, and that pristine silicene-derived states still play a role in shaping the overall electronic structure.

In contrast, the PDOS associated with Al atoms reveals that Al-derived states contribute significantly near the Fermi level. While Al(s) states mainly populate the deeper valence region, the Al(p) orbitals show pronounced weight in the energy range around and across the Fermi level. This strong Al(p)-state contribution near E_F is a key factor driving the transition from semiconducting behavior in pristine hydrogen-passivated SiNRs to semi-metallic behavior in the alloyed system. The hybridization between Al(p) states and Si(p) states results in band crossing and finite density of states at the Fermi level, consistent with semi-metallicity.

Importantly, the PDOS results demonstrate that the electronic states at the Fermi level are not solely derived from the silicene backbone but arise from cooperative Si-Al orbital hybridization, with Al acting as an effective hole donor that shifts the Fermi level into previously gapped regions. This finding provides a microscopic explanation for the electronic transition induced by alloy formation rather than simple rigid-band doping.

Spin-polarized calculations were also performed to examine the possibility of magnetism induced by Al incorporation. No spin splitting or asymmetric spin-resolved density of states was observed, indicating that the 1-1 alloy configuration remains non-magnetic. This suggests that, despite the reduced dimensionality and group-III substitution, Al alloying does not introduce localized magnetic moments in the present system.

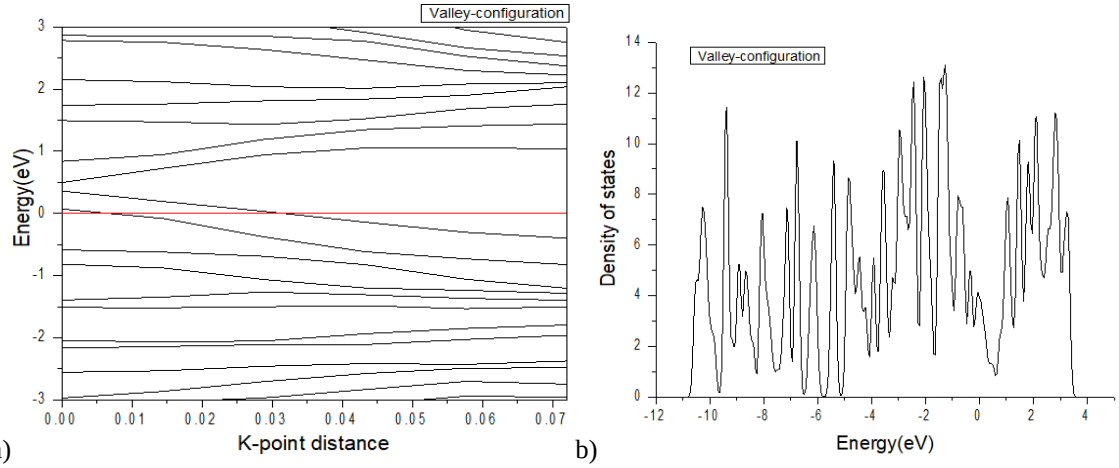

Figure 5. Electronic band structure and density of states of valley doped system

Source: Author, 2025

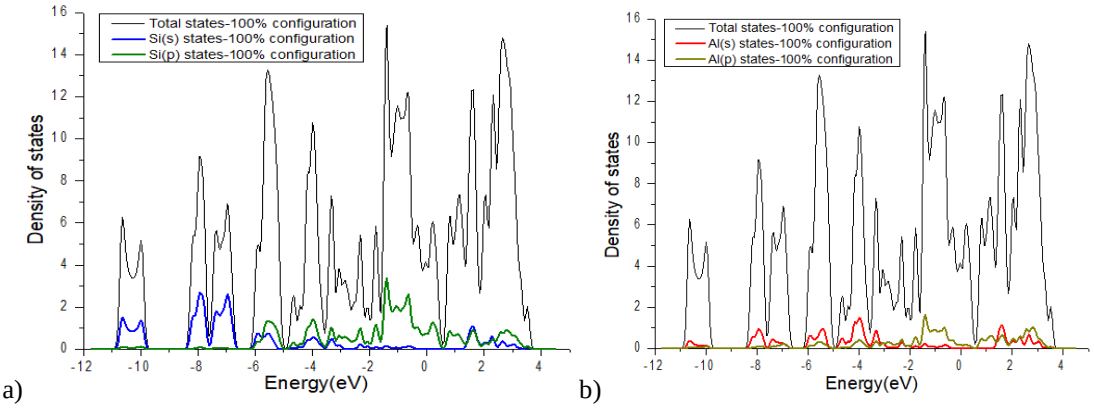

Figure 6. The s, p states in the 1-1 alloy configuration

Source: Author, 2025

For the top configuration, the projected DOS confirms that the semi-metallic character mainly originates from the Si framework, while Al plays a more perturbative role. In the Si-resolved PDOS, the states near the Fermi level (from roughly -2 to 2 eV) are dominated by Si(p) orbitals, whereas Si(s) contributions are mainly located deeper in the valence region (between about -9 and −4 eV). This indicates that the conducting channels are essentially p-like Si states along the ribbon backbone. In contrast, the Al-resolved PDOS shows much smaller spectral weight: Al(s) and Al(p) states appear as weak features in the lower valence band (around -8 to -5 eV) and with only minor intensity close to the Fermi level. The small but finite overlap between Si(p) and Al(p) features reflects a modest Si-Al hybridization, which slightly perturbs the Si bands and shifts the Fermi level into a region with non-zero DOS, driving the transition from a narrow-gap semiconductor (pristine ribbon) to a semi-metal.

For the valley configuration, the projected density of states exhibits trends similar to those observed in the top configuration, with the electronic states near the Fermi level being predominantly derived from the Si backbone. The Si-resolved PDOS shows that Si(s) states mainly occupy the deep valence region below approximately -7 eV, while Si(p) orbitals dominate the energy window close to the Fermi level, particularly between about -3 and 2 eV. These Si(p) states provide the primary contribution to the finite density of states at the Fermi level, indicating that charge transport is largely governed by the silicene nanoribbon framework. In contrast, the Al-derived PDOS displays very weak spectral weight across the entire energy range, with only minor Al(s) and Al(p) contributions appearing in the lower valence region and negligible intensity at the Fermi level. This suggests limited direct involvement of Al orbitals in forming conductive states for the valley configuration. Instead, Al acts mainly as an acceptor-type substitution that modifies the local electronic environment and shifts the Fermi level into Si-derived bands, giving rise to semi-metallic behavior. Consequently, the valley configuration can be described as Si-dominated in terms of electronic transport, with Al inducing an indirect electronic modulation through mild Si-Al hybridization rather than strong band reconstruction.

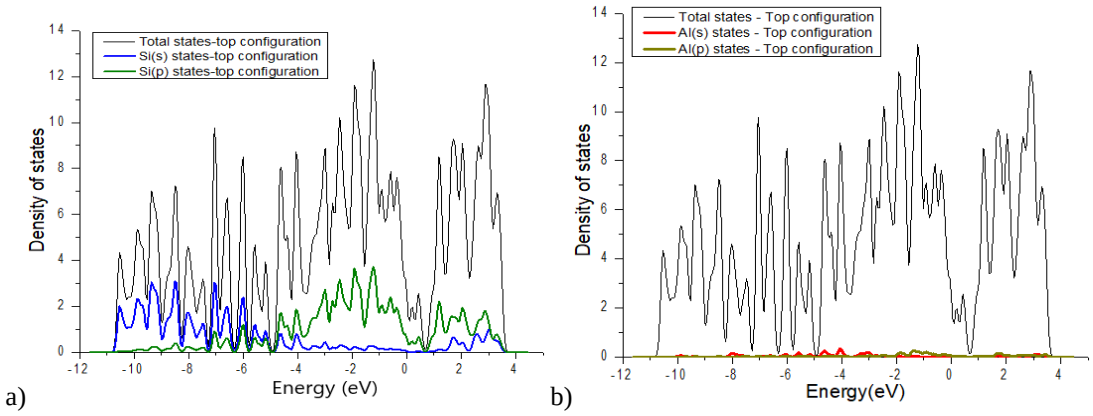

Figure 7. The s, p states in the top doped system

Source: Author, 2025

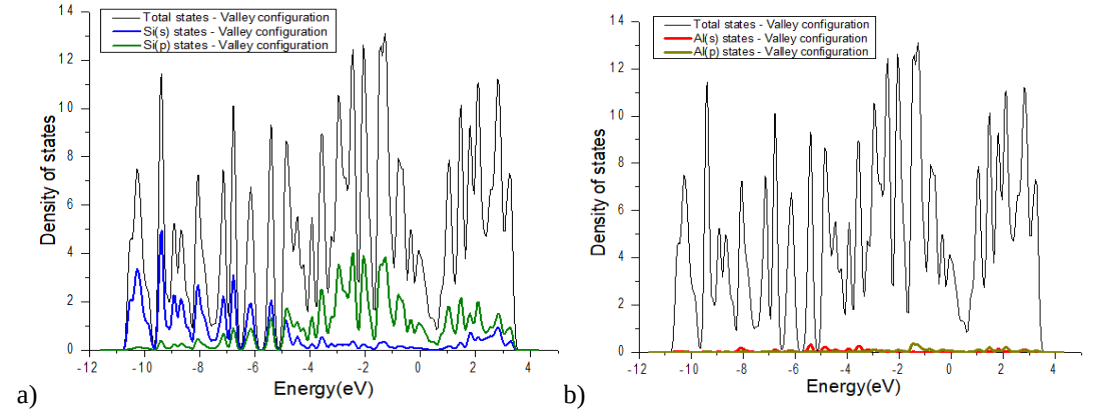

Figure 8. The s, p states in the valley doped system.

Source: Author, 2025

Figures 9a-c illustrate the charge-density distributions for the top, valley, and 1-1 alloy configurations. In these isosurfaces, red regions correspond to areas of high electron density, whereas green regions indicate lower electron-density accumulation. For both the top and valley configurations, the electron density is strongly localized along the Si-Si bonds, reflecting robust σ-bonding typical of the silicene backbone. By contrast, the Si-Al bonds exhibit noticeably weaker charge accumulation, represented by lighter red or yellowish regions. This reduction in electron density is consistent with the electron deficiency introduced by Al, which contains one fewer valence electron than Si, thereby weakening the covalent character of the Si-Al bond.

In the 1-1 alloy configuration, where the doping concentration is significantly higher, the charge density becomes more evenly distributed among the various Si-Al bonds. This indicates a partial redistribution of electrons within the lattice, allowing the system to reach a new equilibrium despite the large number of dopant atoms. However, this configuration also demonstrates structural sensitivity to external perturbations: when the applied electric field is increased to 0.2 eV/Å, the atomic framework becomes unstable, and the Si-Al bonds break. This observation further supports the conclusion that Si-Al bonds are inherently weaker than Si-Si bonds and that the stability of the system is strongly dependent on the magnitude of the applied field.

Figure 9d presents the charge-density difference for the 1-1 alloy configuration, highlighting regions of charge accumulation and depletion. In this representation, yellow zones denote electron accumulation (negative charge), while green zones indicate electron depletion (positive charge). The charge-density difference shows that the electron redistribution is largely local, confined around individual dopant and host atoms. Notably, the Al atoms exhibit greater electron accumulation, reflecting charge transfer from neighboring Si atoms to the more electronegative sites created by doping. Meanwhile, the relatively uniform distribution of positive charge along the interatomic junctions suggests that, despite the high dopant concentration, the system achieves a structurally balanced and energetically stable arrangement at the 50% Al substitution level.

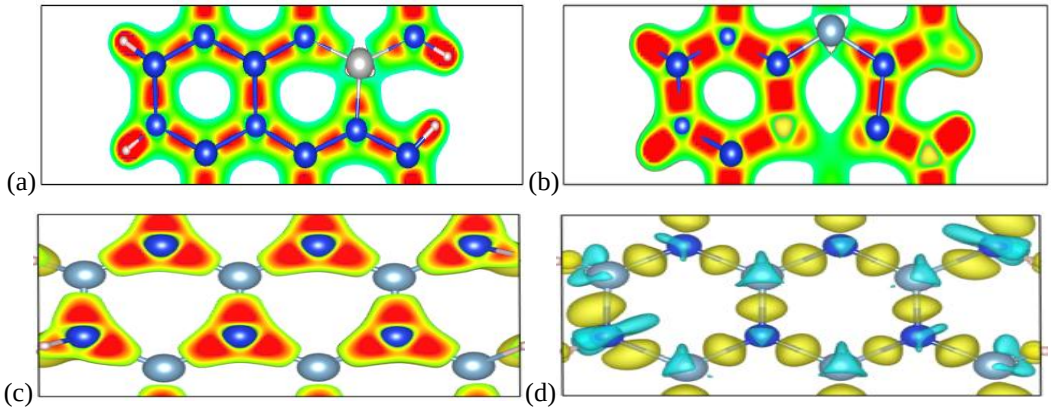

Figure 9. The charge distribution in the top (a), valley (b), 1-1 (c) configurations, and the charge difference in the 1-1 alloy configuration (d)

Source: Author, 2025

4. Conclusion

In this study, we investigated the structural and electronic properties of silicene nanoribbons (SiNRs) doped with aluminum in three representative and energetically stable configurations: the top, valley, and 1-1 substitutional arrangements. Several additional doping geometries were also examined; however, these were found to be structurally unstable, exhibiting significant distortions or complete bond breaking during the relaxation process. Among the stable configurations, the 1-1 alloy structure demonstrates the highest thermodynamic stability, as evidenced by its lowest formation energy. This enhanced stability arises from the symmetric distribution of Al dopants and the resulting balance in the local bonding environment.

The pristine hydrogen-passivated SiNR is a narrow-gap semiconductor, but upon Al incorporation, all three stable doped systems undergo a transition to semi-metallic behavior. This change is driven by the electronic characteristics of aluminum-a group-III element that introduces hole carriers and shifts the Fermi level-thereby enhancing electrical conductivity. The emergence of semi-metallicity across all doping configurations highlights the strong influence of substitutional Al on the electronic structure of silicene nanoribbons. The findings demonstrate that Al doping provides an effective route to modulate the electronic properties of SiNRs, enabling controlled transitions between semiconducting and semi-metallic regimes. Combined with the tunability introduced by an external electric field, this work suggests promising

opportunities for designing novel low-dimensional materials with customizable transport characteristics for future nanoelectronic and optoelectronic applications.

Acknowledgments

This research used resources of the high-performance computer cluster (HPCC) at Thu Dau Mot University (TDMU), Ho Chi Minh City, Vietnam.

References

Takeda, K.; Shiraishi, K. (1994). *Theoretical possibility of stage corrugation in Si and Ge analogs of graphite*. Physical Review B, 50, 14916–14922. https://doi.org/10.1103/PhysRevB.50.14916

Guzmán-Verri, G.; Lew Yan Voon, L. C. (2007). *Electronic structure of silicon-based nanostructures*. Physical Review B, 76, 075131. https://doi.org/10.1103/PhysRevB.76.075131

Cahangirov, S.; Topsakal, M.; Aktürk, E.; Şahin, H.; Ciraci, S. (2009). *Two- and one-dimensional honeycomb structures of silicon and germanium*. Physical Review Letters, 102, 236804. https://doi.org/10.1103/PhysRevLett.102.236804

Lebègue, S.; Eriksson, O. (2009). *Electronic structure of two-dimensional crystals from ab initio theory*. Physical Review B, 79, 115409. https://doi.org/10.1103/PhysRevB.79.115409

Vogt, P.; De Padova, P.; Quaresima, C.; Avila, J.; Frantzeskakis, E.; Asensio, M. C.; et al. (2012). *Silicene: Compelling experimental evidence for graphenelike two-dimensional silicon*. Physical Review Letters, 108, 155501. https://doi.org/10.1103/PhysRevLett.108.155501

Fleurence, A.; Friedlein, R.; Ozaki, T.; Kawai, H.; Wang, Y.; Yamada-Takamura, Y. (2012). *Experimental evidence for epitaxial silicene on diboride thin films*. Physical Review Letters, 108, 245501. https://doi.org/10.1103/PhysRevLett.108.245501

Drummond, N.; Zólyomi, V.; Fal'ko, V. (2012). *Electrically tunable band gap in silicene*. Physical Review B, 85, 075423. https://doi.org/10.1103/PhysRevB.85.075423

Ezawa, M. (2012). *Valley-polarized metals and quantum anomalous Hall effect in silicene*. Physical Review Letters, 109, 055502. https://doi.org/10.1103/PhysRevLett.109.055502

Ding, Y.; Ni, J. (2009). *Electronic structures of silicene nanoribbons: Two-edge-chemistry modification and first-principles study*. Applied Physics Letters, 95, 083115. https://doi.org/10.1186/s11671-016-1584-5

Kara, A.; Enriquez, H.; Seitsonen, A. P.; Voon, L. C. L. Y.; Vizzini, S.; Aufray, B.; Oughaddou, H. (2012). *A review on silicene-New candidate for electronics*. Surface Science Reports, 67, 1–18. https://doi.org/10.1016/j.surfrep.2011.10.001

Kresse, G.; Furthmüller, J. (1996). *Efficient iterative schemes for ab initio total-energy calculations using a plane-wave basis set*. Physical Review B, 54, 11169–11186. https://doi.org/10.1103/PhysRevB.54.11169

Kresse, G.; Joubert, D. (1999). *From ultrasoft pseudopotentials to the projector augmented-wave method*. Physical Review B, 59, 1758–1775. https://doi.org/10.1103/PhysRevB.59.1758

Ezawa, M. (2013). *Monolayer topological insulators: Silicene, germanene, and stanene*. Journal of the Physical Society of Japan, 82, 102001. https://doi.org/10.7566/JPSJ.84.121003